Int. J. Electrochem. Sci., 15 **(2020)** 7001 – 7012, doi: 10.20964/2020.07.81

International Journal of
ELECTROCHEMICAL
SCIENCE
www.electrochemsci.org

Oxygen evolution electrocatalytic properties of perovskite-type oxides obtained by PVP sol-gel route: Part II. The effect of partial substitution of Sm for Sr in $La_{0.4}Sr_{0.6}CoO_3$

Narendra Kumar Singh[*], *Priya Sharma, Manish Kumar Yadav and Reena Parihar*

Department of Chemistry, Faculty of Science, University of Lucknow, Lucknow-226007, India
[*]E-mail: nksbhu@yahoo.com, singh_narendra@lkouniv.ac.in

Received: 9 March 2020 / *Accepted:* 2 May 2020 / *Published:* 10 June 2020

This paper deals the findings of quaternary perovskite-type oxides, $La_{0.4}Sm_xSr_{0.6-x}CoO_3$ ($0 \leq x \leq 0.4$), which is the extended research work obtained by further substitution Sm (0.2 to 0.4 mol) for Sr in the ternary perovskite oxide of $La_{0.4}Sr_{0.6}CoO_3$ prepared by PVP sol-gel route. The cyclic voltammogram (CV) showed similar redox peaks; one anodic an anodic (Ep_a = 489 ± 20 mV) and corresponding cathodic (Ep_c = 355 ± 25 mV) with each oxide electrode in the potential region 0.0-0.7 V. The anodic polarization study in 1 M KOH at 25 ºC indicates that the substitution of Sm (0.2 and 0.3 mol) increased the electrocatalytic property of the material. However, a reduction in electrocatalytic activity is observed with 0.4 mol Sm-substitution. At potential E = 800 mV, $La_{0.4}Sm_{0.2}Sr_{0.4}CoO_3$ (j = 191.9 $mAcm^{-2}$) showed about 5 times higher electrocatalytic activity than base oxide; $La_{0.4}Sr_{0.6}CoO_3$ (j = 37.6 $mAcm^{-2}$). A reduction in Tafel slope has also been observed upto 0.3 mol Sm-substitution. Similar trend was also found in the case of thermodynamic study, such as standard entropy of activation ($\Delta S^{\circ\#}$), standard enthalpy of activation ($\Delta H^{\circ\#}$) and standard electrochemical energy of activation ($\Delta H_{el}^{\circ\#}$) of the materials. Some physicochemical techniques like X-ray diffraction (XRD) and scanning electron microscope (SEM) have been used to analyze the synthesized products.

Keywords: Quaternary perovskite-type oxides, PVP method, XRD, Electrocatalytic activity, Thermodynamic parameters

1. INTRODUCTION

La-based perovskite-type mixed oxides with Co-, Mn- and Ni- are considered as very promising materials for several technological process [1-3] and have been extensively studied for oxygen evolution/reduction reaction [1, 4-25]. Earlier, these oxides were prepared by solid state reaction and thermal decomposition method. Oxides produced by these methods [26-31] required relatively high temperature and produced oxide powders with low specific surface area and reduced homogeneity.

Recently, Singh et al. adopted low temperature reported methods [32-35] for the synthesis of La-based perovskite oxides and found considerable improvement in the physicochemical as well as electrochemical properties of these oxides. Amorphous organic acids, like malic acid (MA), citric acid (CA), polyacrylic acid (PAA), citric acid-ethylene diamine (CA-EDA) etc used in these methods facilitate to give the homogeneity in the metal ions and therefore produced oxides relatively at lower temperature.

Recently, we produced lanthanum cobaltate perovskite-type oxides and their Sr and Cu-substituted products by using low temperature sol-gel routes [36-38] and studied their electrocatalytic properties towards OER. Oxygen evolution electrocatalytic properties of some perovskite mixed oxides of La with Fe have also been reported in literature [39, 40] during recent years. Azad et al. [40] used perovskite oxides as bifunctional electrocatalysts with oxygen evolution current density 10 mA cm^{-2} at E = 1.65 V vs RHE. Fe-doped $LaNiO_3$ electrocatalysts have been developed by Júlio C. Sczancoski et al. [41] and studied OER on deposited on pyrolytic graphite sheets and found the highest electrocatalytic activity for $LaNi_{0.4}Fe_{0.6}O_3$ with Tafel slope value of 52 mV $decade^{-1}$. The findings of these articles revealed that the preparation method, precursors used in the synthesis, metal ion substitution, pH of the solution and preparation temperature strongly affected the electrocatalytic properties.

Shao-Horn et al. [42] from Massachusetts Institute of Technology, USA used elements of lanthanide series instead of La and prepared double perovskites $(Ln_{0.5}Ba_{0.5})CoO_{3-\delta}$ (Ln = Pr, Sm, Gd and Ho) by adopting thermal decomposition method and found better electrocatalytic activity towards oxygen evolution reaction in alkaline solution. Also, literature showed that perovskites with Sm have very little been investigated with regards to oxygen evolution/reduction reaction.

In view of these, we planned to extend the research work and synthesized quaternary perovskite oxides by substituting Sm for Sr in $La_{0.4}Sr_{0.6}CoO_3$ oxide lattice which is recently obtained by polyvinylpyrrolidone (PVP) sol-gel route [38]. Results of the study, so obtained, are described in this paper.

2. EXPERIMENTAL

Quaternary perovskite-type oxides, $La_{0.4}Sm_xSr_{0.6-x}CoO_3$ ($0 \leq x \leq 0.4$) have been prepared by adopting the method reported elsewhere [38, 43]. Nitrate salt of metals *viza.* $Sm(NO_3)_3.6H_2O$ (Merck, 99.9%), $La(NO_3)_3.6H_2O$ (Himedia, 99.0%), $Co(NO_3)_3.6H_2O$ (Merck, 98%), $Sr(NO_3)_2$ (Merck, 99.0%) with high purity was taken as starting material. So, no further purification has been done for the preparation of oxides. As per stoichiometry of the oxides, nitrate salt of metals was weighed and prepared an aqueous solution in double distilled water. Further, polyvinylpyrrolidone (Sigma-Aldrich, Molecular Wt. 40,000) with ratio, PVP: 3 times the total moles of cations, was added to this solution. The mixture was then evaporated on water bath with constant stirring. A gel like mass was obtained which decomposed at higher temperature. This polymerized precursor was then sintered at 600 ºC for 5 hrs in a PID controlled electrical furnace (ASCO, India) to get the desired oxides.

An XPERT-PRO Diffractometer (Model PW3050/60) provided with radiation Source Cu-Kα (λ = 1.54048 Å) was used to determine the perovskite phase of the synthesized materials. The crystallite

size of the material was estimated by using Scherrer's formula. The morphological study of oxide powder was done by scanning electron microscope (JOEL JSM 6490LV).

Similar to the ternary perovskite oxides, all the electrochemical properties have been performed in three electrode single compartment glass cell. In the experimental setup, the oxide film electrode on Ni-substrate was taken as the working electrode. A platinum foil (area ~2 cm^2) and Hg/HgO/1M KOH (E° = 0.098 V vs NHE at 25°C) were used as auxiliary and reference electrode, respectively. The cleaning of Ni-foil, preparation of oxide film on Ni-support and formation of oxide film electrode were performed in the similar way as mentioned in the literature [11, 17]. An electrochemical workstation (Gamry Reference 600 ZRA) provided with potentiostat/galvanostat and corrosion & physical electrochemistry software was used to run the electrochemical experiments. The data was recorded and stored on the desktop computer (HP) connected to the electrochemical workstation. A Luggin capillary (agar-agar and potassium chloride gel) was used to minimize the ohmic resistance (iR drop).

3. RESULT AND DISCUSSION

3.1 Physicochemical Properties

3.1.1 Scanning Electron Micrograph (SEM)

The scanning electron micrographs of samarium substituted quaternary oxide powder, sintered at 600°C for 5 hrs, are shown in Fig. 1 at the magnification ×1500.

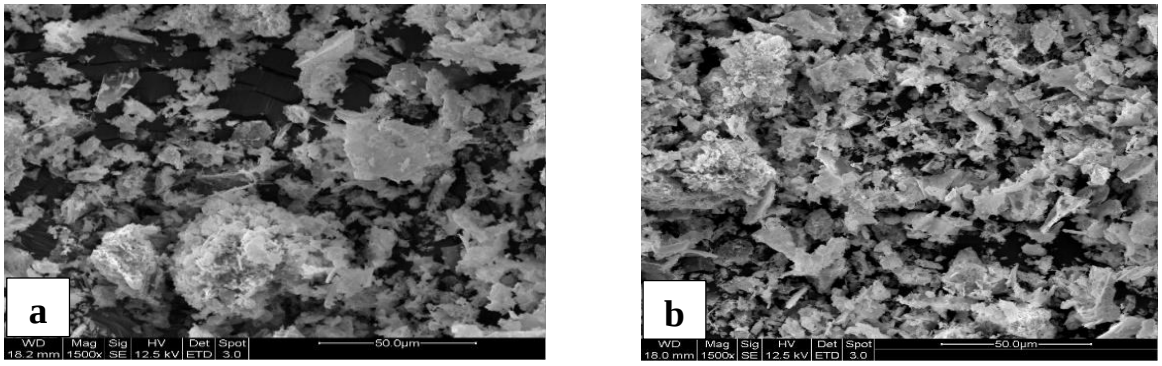

Figure 1. SE Micrographs of oxide powder sintered at 600 ˚C for 5 h; a: $La_{0.4}Sm_{0.2}Sr_{0.4}CoO_3$, b: $La_{0.4}Sm_{0.3}Sr_{0.3}CoO_3$

The morphology of the oxide is observed to be similar to that found in the case of ternary perovskite oxides [38] and appears to be flakes like structure.

3.1.2 X-ray diffraction (XRD)

Fig. 2 shows the powder X-Ray diffraction patterns of oxide powders, $La_{0.4}Sm_{0.2}Sr_{0.4}CoO_3$ and $La_{0.4}Sm_{0.4}Sr_{0.2}CoO_3$, sintered at 600 ºC for 6h, in 2θ = 20° to 100°.

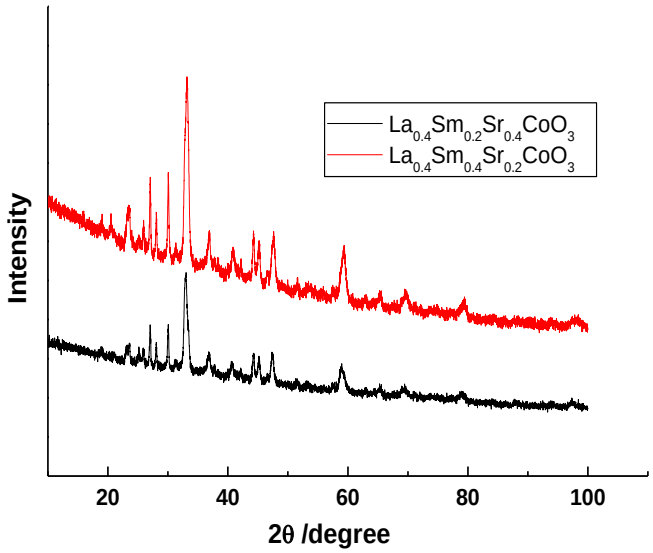

Figure 2. XRD powder patterns of oxide powder sintered at 600 ˚C for 5 h

Values of 2θ and 'd' corresponding to each diffraction lines were found to be very close to their respective JCPDS ASTM file 25-1060 and followed hexagonal crystal geometry. The observed data shows that the materials produced have almost perovskite phase. The Scherer's formula [44], S = 0.9λ/BCosθ, was used to calculate the crystallite size of the material and found to be ~35 nm and ~50 nm $La_{0.4}Sm_{0.2}Sr_{0.4}CoO_3$ and $La_{0.4}Sm_{0.4}Sr_{0.2}CoO_3$ oxide, respectively.

3.2. Electrochemical properties

3.2.1. Cyclic Voltammetry (CV)

Figure 3 represents the CV curve of the oxide film electrode on Ni-substrate, recorded in 1 M KOH at 25 °C. The substitution of Sm for Sr did not affect the nature of the voltammetric curve obtained with each oxide electrode and produced an anodic (Ep_a = 489 ± 20 mV) and corresponding cathodic (Ep_c = 355 ± 25 mV) peak in the potential region 0.0 - 0.7 V. Values of cyclic voltammetric parameters, so estimated, are listed in Table 1.

As reported earlier [45], these values of redox potential correspond to the redox potential of bare Ni. Since oxides are prepared at very low temperature the hydration of the oxide film may easily possible in contact with the solution during electrolysis process.

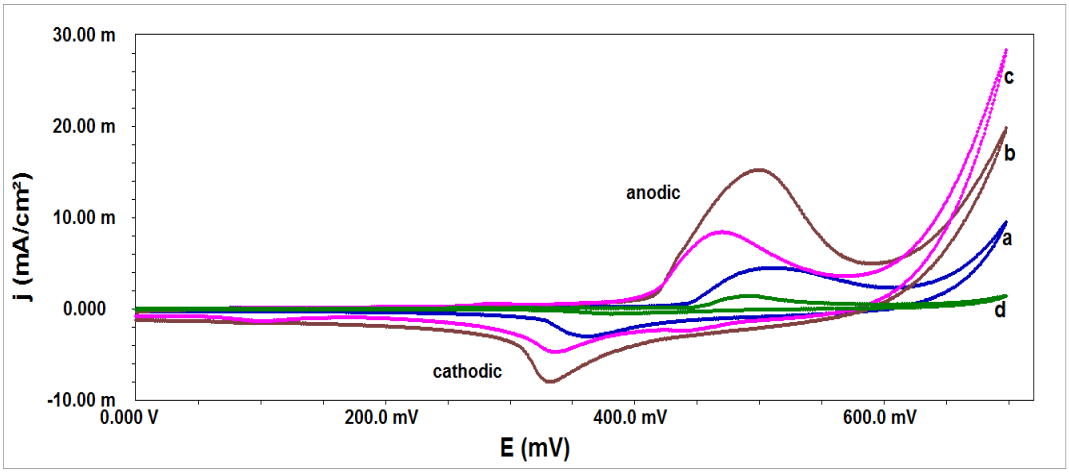

Figure 3. Cyclic voltammograms of Ni/$La_{0.4}Sm_xSr_{0.6-x}CoO_3$ ($0 \leq x \leq 0.4$) in 1M KOH at 25˚C; (SR = 20 mV sec^{-1}), a: $La_{0.4}Sr_{0.6}CoO_3$, b: $La_{0.4}Sm_{0.3}Sr_{0.3}CoO_3$, c: $La_{0.4}Sm_{0.4}Sr_{0.2}CoO_3$, d: $La_{0.4}Sm_{0.2}Sr_{0.4}CoO_3$

Table 1. Values of the cyclic voltammetric parameters on $La_{0.4}Sm_xSr_{0.6-x}CoO_3$ ($0 \leq x \leq 0.4$) in 1 M KOH at 25°C (scan rate = 20 mVsec^{-1}):

Electrode	E_{Pa} (mV)	E_{Pc} (mV)	ΔE_p (mV)	$E^\circ = (E_{Pa}+E_{Pc})/2$ (mV)	$\|j_{Pa}\|$ /mA cm^{-2}	$\|j_{Pc}\|$ /mA cm^{-2}	$\|j_{Pa}\| / \|j_{Pc}\|$	q /mC cm^{-2}
$La_{0.4}Sr_{0.6}CoO_3$	509	361	148	435	4.5	3.1	1.5	55.5
$La_{0.4}Sm_{0.2}Sr_{0.4}CoO_3$	469	336	133	402	8.4	4.8	1.8	101.8
$La_{0.4}Sm_{0.3}Sr_{0.3}CoO_3$	499	331	168	415	15.2	8.0	1.9	165.9
$La_{0.4}Sm_{0.4}Sr_{0.2}CoO_3$	491	380	111	435	1.4	0.6	2.3	11.9

The study of variation in redox potential with scan rate has also been done with each oxide electrode in 1M KOH at 25°C. A representative CV curve for the Ni/$La_{0.4}Sm_{0.4}Sr_{0.2}CoO_3$ is shown in the Fig. 4. As observed in the case of ternary perovskite oxides, both anodic and cathodic peak potential shifted either side when scan rate increases from 20 to 120 mV sec^{-1}. The observed shifts seem to be 68-120 mV and 6-34 mV towards anodic and cathodic region, respectively. The ratio of anodic and cathodic peak current is more than unity, which indicates the irreversible nature [46-48] of the redox process. The anodic and cathodic peak currents are plotted against square root of scan rate and represented in Fig. 5 for the oxide electrode $La_{0.4}Sm_{0.2}Sr_{0.4}CoO_3$. The voltammetric charge (q), which is determined by integrating the CV curve upto the potential just prior to the start of oxygen evolution reaction, is plotted against (scan rate)$^{-1/2}$ for each oxide electrode and shown in Fig. 6. The straight line obtained in both figures specifies the diffusion-controlled process [17] of the redox couple.

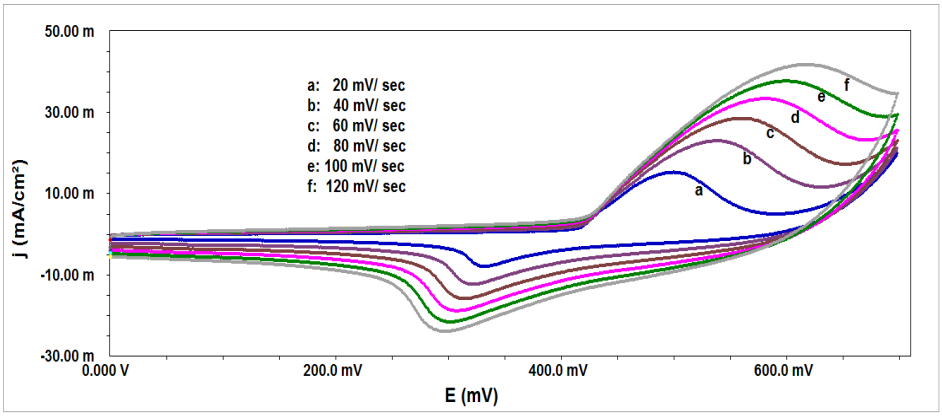

Figure 4. Cyclic voltammogram of $Ni/La_{0.4}Sm_{0.4}Sr_{0.2}CoO_3$ at different scan rates in 1M KOH at 25˚C

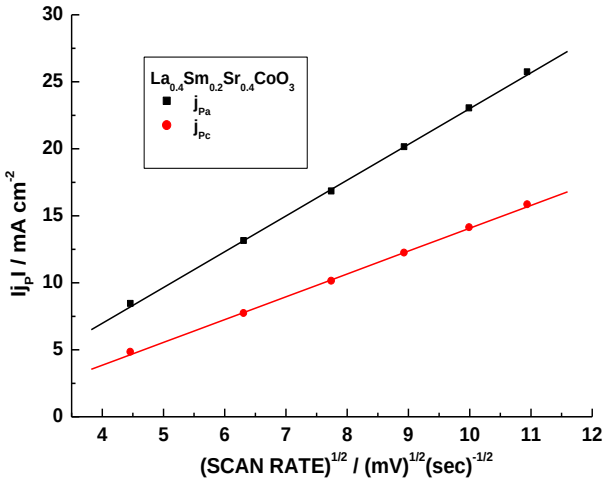

Figure 5. Plot of $|j_P|$ vs (scan rate)$^{1/2}$ for $Ni/La_{0.4}Sm_{0.4}Sr_{0.2}CoO_3$ film electrodes on Ni in 1M KOH (25°C)

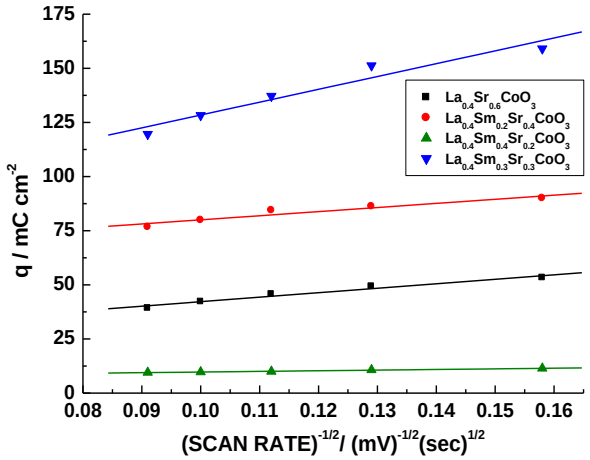

Figure 6. Plot of voltammetric charge (q) vs (scan rate)$^{-1/2}$ for the oxide film electrodes on Ni in 1M KOH (25°C)

3.2.2. Electrocatalytic activity

The effect of Sm-substitution on the electrocatalytic activity of $La_{0.4}Sr_{0.6}CoO_3$ has been determined by recording iR-compensated anodic polarization curve (E vs log j) in 1M KOH at 25 °C, recorded at a slow scan rate of 0.2 mV sec^{-1}. The polarization curve for each oxide electrode is shown in Fig. 7. The Tafel slope and electrocatalytic activity have been determined by estimating the polarization curve and shown in the Table 2. From figure 7 and table 2 it is observed that substitution of 0.2 and 0.3 mol Sm (191.9 and 144.6 mA cm^{-2} at 800 mV) increases the electrocatalytic activity. The Tafel slope values are also found to decrease with these oxide electrodes (~ 65 mV $decade^{-1}$). Further, substitution of 0.4 mol Sm increases the Tafel slope (110 mV $decade^{-1}$) value thereby decreasing the electrocatalytic activity (14.9 mA cm^{-2} at 800 mV). However, in the higher potential region, polarization of these oxides electrodes takes place and therefore, a very high Tafel slope value has been observed.

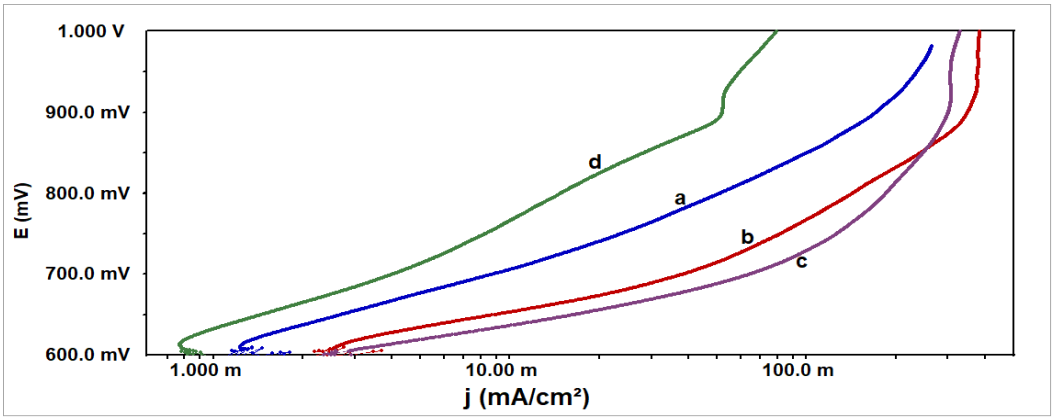

Figure 7. Anodic polarization curve for Ni/$La_{0.4}Sm_xSr_{0.6-x}CoO_3$ ($0 \leq x \leq 0.4$) film electrodes in 1M KOH (25°C); (scan rate = 0.2 mVsec^{-1}), a: $La_{0.4}Sr_{0.6}CoO_3$, b: $La_{0.4}Sm_{0.3}Sr_{0.3}CoO_3$, c: $La_{0.4}Sm_{0.2}Sr_{0.4}CoO_3$, d: $La_{0.4}Sm_{0.4}Sr_{0.2}CoO_3$

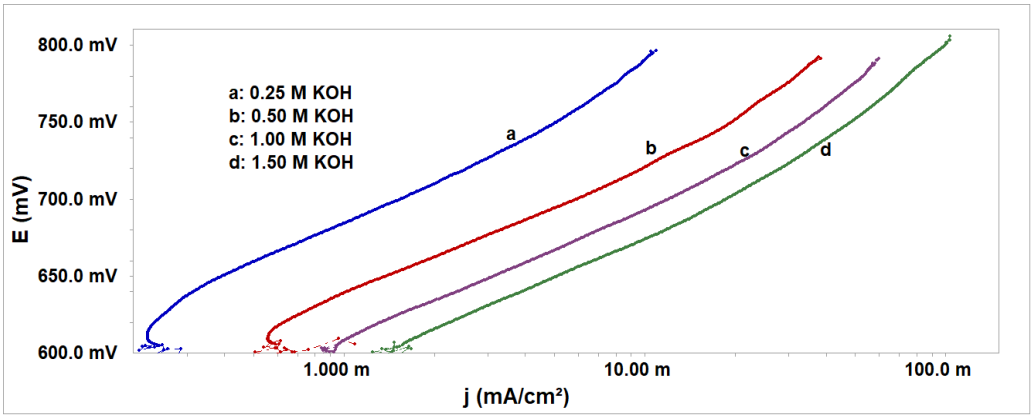

Figure 8. Anodic polarization curve for Ni/ $La_{0.4}Sm_{0.2}Sr_{0.4}CoO_3$ at different KOH concentrations (μ = 1.5) at 25 ˚C

Further, electrode kinetic study has been extended to determine the order of oxygen evolution reaction. For the purpose, anodic polarization curve was recorded with each oxide electrode in different KOH concentrations at 25 °C. In order to maintain the electrical intensity uniform, the ionic strength of the solution was maintained 1.5 by using inert electrolyte KNO_3. The polarization curve of electrocatalysts in varying KOH concentrations was observed to similar. A representative curve for Ni/ $La_{0.4}Sm_{0.2}Sr_{0.4}CoO_3$ is shown in the Fig. 8. From the polarization curve, the current density (in A cm^{-2}) data was collected at a certain potential (E = 700 mV). A plot log j vs. log [OH^-], as shown in the Fig. 9, was constructed for each oxide electrode. The order of reaction was estimated by measuring the slope of straight line and given in Table 2. The fractional order of reaction obtained with each electrocatalyst is very common and it has already been reported in literature. The observed values of Tafel slope and reaction order suggest that the OER taking place at the electrocatalysts follows different mechanistic path.

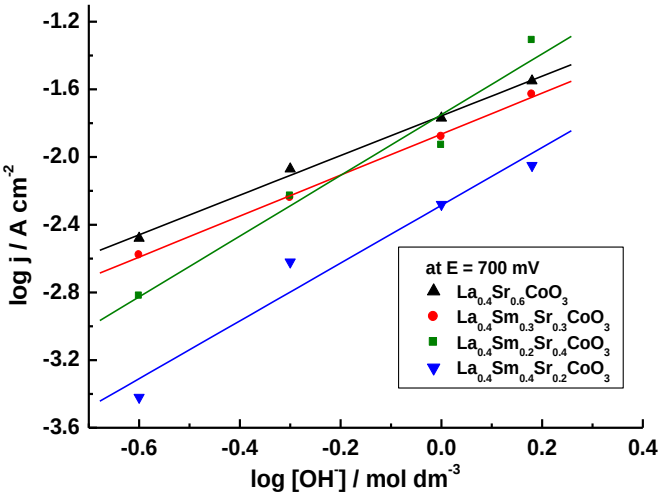

Figure 9. Plot of log j vs log [OH^-] for Ni/$La_{0.4}Sm_xSr_{0.6-x}CoO_3$ ($0 \leq x \leq 0.4$) film electrodes

The electrocatalytic activity of the most active oxide electrode, $La_{0.4}Sm_{0.2}Sr_{0.4}CoO_3$, in the present study has been found to more active as compared those reported in literature [19-22, 37, 49, 50]. The oxide, $La_{0.4}Sm_{0.2}Sr_{0.4}CoO_3$, produced current density (100 mA cm^{-2}) at potential 730 mV. At this current density, $La_{0.8}Sr_{0.2}MnO_3$ obtained by malic acid sol-gel route [20], $La_{0.6}Sr_{0.4}MnO_3$ prepared by citric acid sol-gel route [19], $La_{0.6}Sr_{0.4}MnO_3$ prepared by polyacrylic acid sol-gel route [22] and $La_{0.7}Sr_{0.3}MnO_3$ prepared by CA-EDA sol-gel route [21], contributed 816, 822, 828 and 780 mV, respectively. The $La_{0.7}Sr_{0.3}MnO_3$ obtained by auto combustion method [49] produced 2 mA cm^{-2} at 750 mV in 1M LiOH. Zhang et al. [50] synthesized $La_{0.2}Sr_{0.8}MnO_3$ by sol-gel method and found OER current density 152 mA cm^{-2} at 700 mV in 6M KOH solution. On the other hand, perovskite oxides obtained by some other low temperature methods [17, 36, 51] showed better electrocatalytic activity as compared to the most active electrode of the present study.

Table 2. Electrode kinetic parameters for oxygen evolution reaction on $La_{0.4}Sm_xSr_{0.6-x}CoO_3$ ($0 \leq x \leq 0.4$) in 1 M KOH at 25°C

Electrode	Tafel slope / mVd^{-1}	Order (p)	E/ mV at j (mA cm^{-2})		j (mA cm^{-2}) at E/mV		
			10	100	700	750	800
$La_{0.4}Sr_{0.6}CoO_3$	71	1.2	728	857	5.4	16.3	37.6
$La_{0.4}Sm_{0.2}Sr_{0.4}CoO_3$	64	1.8	638	730	63.6	129.9	191.9
$La_{0.4}Sm_{0.3}Sr_{0.3}CoO_3$	65	1.2	656	767	37.6	82.6	144.0
$La_{0.4}Sm_{0.4}Sr_{0.2}CoO_3$	110	1.7	765	1042	3.9	8.3	14.9

3.2.3. Thermodynamic Parameters

Thermodynamic parameters, such as standard entropy of activation ($\Delta S^{\circ\#}$), standard enthalpy of activation ($\Delta H^{\circ\#}$) and standard electrochemical energy of activation ($\Delta H_{el}^{\circ\#}$) have been calculated by recording the anodic polarization in 1M KOH at varying temperature. A representative polarization curve for $La_{0.4}Sm_{0.2}Sr_{0.4}CoO_3$ is shown in Fig. 10. At a constant potential, current is measured from the polarization curve recorded at each temperature ant plotted against 1/T (Fig. 11). The value of $\Delta H_{el}^{\circ\#}$ was estimated from the slope of straight-line at potential, E = 700 mV.

Further, following two relations (1) and (2) [38, 52] are used to calculate the standard enthalpy of activation ($\Delta H^{\circ\#}$) and standard entropy of activation ($\Delta S^{\circ\#}$), respectively.

$$\Delta H_{el}^{\circ\#} = \Delta H^{\circ\#} - \alpha F\eta \quad \ldots. (1)$$

$$\Delta S^{\circ\#} = 2.3R\,[\log j + \Delta H_{el}^{\circ\#}/2.3RT - \log (nF\omega C_{OH^-})] \quad \ldots(2)$$

In equation (1), α (= 2.303RT/bF) is the transfer coefficient, where R, F and T are the gas constant, Faraday constant and absolute temperature, respectively. 'b' is the Tafel slope (in mV $decade^{-1}$) determined from the polarization curve recorded at different temperature.

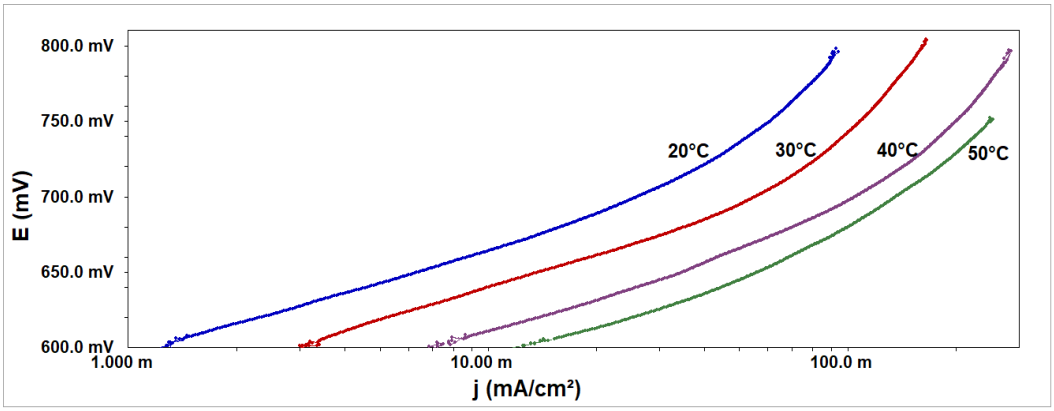

Figure 10. Anodic polarization curve on $Ni/La_{0.4}Sm_{0.2}Sr_{0.4}CoO_3$ in 1M KOH at varying temperature

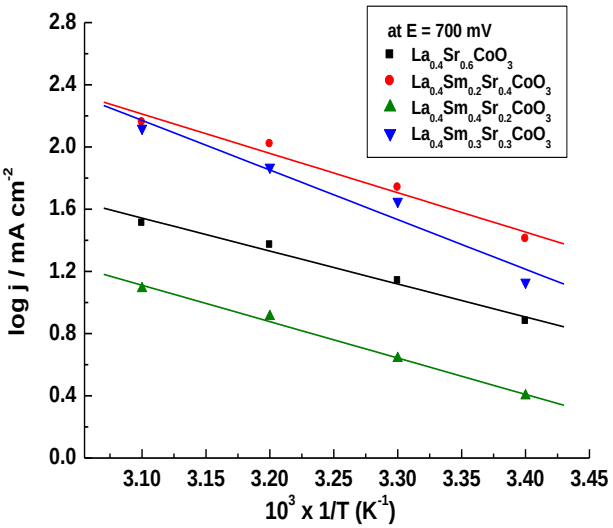

Figure 11. The Arrhenius plot for Ni/$La_{0.4}Sm_xSr_{0.6-x}CoO_3$ ($0 \leq x \leq 0.4$) film electrode in 1M KOH

The overpotential (η) is determined by the relation $\eta = E - E_{O2/OH^-}$, where E and E_{O2/OH^-} (= 0.303 V vs. Hg/HgO) are the applied potential [38, 53] across the catalyst/ 1 M KOH interface and the theoretical equilibrium Nernst potential in 1 M KOH at 25 ˚C, respectively. In equation (2), all the terms have their usual meaning. The frequency term ω (= k_BT/h) where, k_B and h are the Boltamann constant and Plank's constant, respectively. Values of all the thermodynamic parameters are shown in Table 3. As expected, the value of $\Delta H_{el}^{\circ\#}$ was found to be minimum (39.9 kJ mol^{-1}) with most active electrode, $La_{0.4}Sm_{0.2}Sr_{0.4}CoO_3$. The value of $\Delta S^{\circ\#}$ was found to highly negative which suggests the adsorption phenomena in the oxygen evolution reaction.

Table 3. Thermodynamic parameters for O_2 evolution on $La_{0.4}Sm_xSr_{0.6-x}CoO_3$ ($0 \leq x \leq 0.4$) in 1 M KOH

Electrode	$\Delta H_{el}^{o\neq}$ (KJ mol^{-1}) at E = 675 mV	$-\Delta S^{o\neq}$ (J deg^{-1} mol^{-1})	α	$\Delta H^{o\neq}$ (KJ mol^{-1})
$La_{0.4}Sr_{0.6}CoO_3$	66.4	111.7	0.7	89.8
$La_{0.4}Sm_{0.2}Sr_{0.4}CoO_3$	39.9	181.0	0.8	71.3
$La_{0.4}Sm_{0.3}Sr_{0.3}CoO_3$	43.8	188.7	0.6	68.4
$La_{0.4}Sm_{0.4}Sr_{0.2}CoO_3$	51.8	146.0	0.7	79.9

4. CONCLUSION

Findings of the above study indicates that the partial substitution of Sr by Sm in the oxide lattice of $La_{0.4}Sr_{0.6}CoO_3$ enhances the electrocatalytic activity of the material significantly. It is found to be better upto 0.3 mol Sm-substitution. Higher substitution (0.4 mol) deactivated the material and a very high Tafel slope (114 mV $decade^{-1}$) with low activity (14.9 mA cm^{-2} at 800 mV) is observed.

Morphology of the oxide is not affected by the Sm-substitution as almost similar flakes like structure is observed for the oxides with and without samarium.

ACKNOWLEDGEMENTS
Authors are thankful to Department of Chemistry, Lucknow University, Lucknow for providing basic infrastructure and BSIP, Lucknow for SEM analyses. One of the author N. K. Singh is thankful to Department of Science and Technology (DST), New Delhi for electrochemical work station under Fast Track Scheme for Young Scientist (No.: SR/FT/CS–044/2009).

References

1. D. B. Meadocroft, *Nature*, 226 (1970) 847.
2. A.C.C. Tseung & H.L. Bevan, *J. Electroanal. Chem*., 45 (1973) 429.
3. K. Matsuki & H Kamada, *Research on Energy Conversion and Storage Through Chemical Process*, SPEY, vol. 13, 1985, p. 181.
4. Y. Matsumoto & E. Sato, *Electrochim. Acta*, 24 (1979) 421.
5. Y. Matsumoto, S. Yamada, T. Nishida & E. Sato, *J. Electrochem. Soc*., 127 (1980) 2360.
6. S. Yamada, Y. Matsumoto & E. Sato, *The journal of the Electrochemical Society of Japan*, 49 (1981) 269.
7. A.G.C. Kobussen, H. Willems & G.H.J. Broers, *J. Electroanal. Chem*., 142 (1982) 67.
8. J. O'M Bockris, T. Otagawa & V. Young, *J. Electroanal. Chem*., 150 (1983) 633.
9. Y. Shimizu, H. Matsuda, N. Miura & N. Yamazoe, *Chem. Lett*., 21 (1992) 1033.
10. T. Schmidt & H. Wendt, *Electrochim. Acta*., 39 (1994) 1763.
11. S. K. Tiwari, P. Chartier & R. N. Singh, *J. Electrochem. Soc*., 143 (1995) 148.
12. A. N. Jain, S. K. Tiwari, R. N. Singh & P. Chartier, *J. Chem. Soc. Faraday Trans*., 91 (1995) 1871.
13. R. N. Singh, L. Bahadur, J. P. Pandey, S. P. Singh, P. Chartier & G. Poillerat, *J. Appl. Electrochem*, 24 (1994) 149.
14. S. P. Singh, R. N. Singh, G. Poillerat & P. Chartier, *Int. J. Hydrogen Energy*, 20 (1995) 203.
15. R. N. Singh, A. N. Jain, S. K. Tiwari, G. Poillerat & P. Chartier, *J. Appl. Electrochem*., 25 (1995) 1133.
16. S. K. Tiwari, J. F. Koenig, G. Poillerat, P. Chartier & R. N. Singh, *J. Appl. Electrochem*., 28 (1998) 114.
17. R. N. Singh, S. K. Tiwari, S. P. Singh, N. K. Singh, G. Poillearat & P. Chartier, *J. Chem. Soc. Faraday Trans*., 92(14) (1996) 2593.
18. R. N. Singh, S. K. Tiwari, S. P. Singh, A. N. Jain & N. K. Singh, *Int. J. Hydrogen Energy*, 22 (1997) 557.
19. T. Sharma, N. K. Singh, S. K. Tiwari & R. N. Singh, *Ind. J. Engg. & Mat. Sci.*, 5 (1998) 38.
20. N. K. Singh, S. K. Tiwari & R. N. Singh, *Int. J. Hydrogen Energy*, 23 (1998) 775.
21. B. Lal, N. K. Singh & R. N. Singh, *Ind. J. Chem*., 40 A (2001)1269.
22. N. K. Singh, B. Lal & R. N. Singh, *Int. J. Hydrogen Energy*, 27 (2002) 885.
23. B. Lal, M. K. Raghunanda, M. Gupta & R. N. Singh, *Int. J. Hydrogen Energy*, 30 (2005) 723.
24. J. Suntivich, H. A. Gasteiger, N. Yabuuchi, H. Nakanish, J. B. Goodenough & Y. Shao-Horn, *Nature Chemistry*, 3 (2011) 647.
25. J. Sunarso, A.A.J. Torriero, W. Zhou, P.C. Howlett & M. Forsyth, *J. Phys. Chem*., 116 (2012) 5827.
26. J. O. M. Bockris & T. Otagawa, *J. Electrochem. Soc*., 131 (1984) 290.
27. J. Balej, *Int. J. Hydrogen Energy*, 10 (1985) 89.

28. A. G.C. Kobussen, F. R. van Buren, T. G. M. van Den Belt & H. J. A van Wees, *J. Electroanal Chem*., 96 (1979) 123.
29. Y. Matsumotp, H. Manabe & E. Sato, *J. Electrochem Soc*. 123 (1980) 811.
30. H. Wendt & V. Plzak, *Electrochim Acta*, 28 (1983) 27.
31. G. Fiori & C. M. Mari, *Int. J. Hydrogen Energy*, 7 (1982) 489.
32. K. Vidyasagar, J. Gopalkrishnan & C.N.R. Rao, *J. Solid State Chem*., 59 (1985) 29.
33. J. K. Vassiliou, M. Hornbostel, R. Ziebarth & F. J. Disalvo, *Solid State Chem.*, 81 (1989) 208.
34. Y. Teraoka, H. Kakebayashi, I. Moriguchi & S. Kagawa, *Chem Letters*, 20 (1991) 673.
35. H. Taguchi, H. Yoshioka, D. Matsuda & M. Nagao, *Solid State Chem*., 104 (1993) 460.
36. M. K. Yadav, Ritu Yadav, Priya Sharma & N. K. Singh, *Int. J. Electrochem. Sci*., 11 (2016) 8633.
37. N. K. Singh, M. K. Yadav & Carlos Fernandez, *Int. J. Electrochem Sci*., 12 (2017) 7128.
38. N. K. Singh, P. Sharma, I. Kumar & A. S. Chaddha, *Int. J. Electrochem. Sci*., 14 (2019) 11379.
39. Ravi Sankannavar & A. Sarkar, *Int. J. Hydrogen Energy*, 43 (2018) 4682.
40. Uday Pratap Azad, Monika Singh, Sourav Ghosh, Ashish Kumar Singh, Vellaichamy Ganesan, Akhilesh Kumar Singh & Rajiv Prakash, *Int. J. Hydrogen Energy*, 43 (2018) 20671.
41. Cipriano B. Gozzo, Mario R. S. Soares, Júlio C. Sczancoski, Içamira C. Nogueira & Edson R. Leite, *Int. J. Hydrogen Energy*, 39 (2019) 21659.
42. Alexis Grimaud, Kevin J. May, Christopher E. Carlton, Yueh-Lin Lee, Marcel Risch, Wesley T. Hong, Jigang Zhou & Yang Shao-Horn, *Nature Communications*, 4 (2013) 1.
43. T. Nagai, N. Fujiwara, M. Asahi, Shin-ichi Yamazaki, Z. Siroma, T. Ioroi, *J. Asian Ceramic Society*, 2 (2014) 329.
44. N. Fradette & B. Marsan, *J. Electrochem. Soc*., 145 (1998) 2320.
45. N. K. Singh, S. K. Tiwari, K. L. Anitha & R. N. Singh, *J. Chem. Soc. Faraday Trans.*, 92(13) (1996) 2397.
46. Wei Wu, Shaoqiang Guo & Jinsuo Zhang, *Int. J. Electrochem. Sci*., 13 (2018) 225.
47. L. Massot, P. Chamelot, L. Cassayre & P. Taxil, *Electrochim. Acta*, 54 (2009) 6361.
48. A.J. Bard & L.R. Faulkner, *Electrochemical Methods: Principles and Applications, 2nd ed*., Wiley, (2001) New York.
49. Boyoon Shin, Sangwon Choi & Yongsug Tak, *Int. J. Electrochem. Sci*., 11 (2016) 5900.
50. Zejie Zhang, Debi Zhou, Xuewen Wu, Xinjun Bao, Jingjing Liao & Meisheng Wen, *Int. J. Hydrogen Energy*, 44 (2019) 7222.
51. R. N. Singh & B. Lal, *Int. J. Hydrogen Energy*, 27 (2002) 45.
52. E. Gileadi, *Electrode Kinetics*, (VCH Publishers Inc., New York), 1993 p.151
53. R. N. Singh, J. P. Pandey, N. K. Singh, B. Lal, P. Chartier & J. F. Koenig, *Electrochim. Acta*, 45 (2000) 1911.